Eur. Phys. J. D **29**, 195–199 (2004)
DOI: 10.1140/epjd/e2004-00043-1

THE EUROPEAN PHYSICAL JOURNAL D

Lifetimes of metastable levels in Ar II

P. Schef[1], A. Derkatch[1], P. Lundin[1], S. Mannervik[1,a], L.-O. Norlin[2], D. Rostohar[3], P. Royen[1], and E. Biémont[4]

[1] Physics Dept. Stockholm University, AlbaNova, 10691 Stockholm, Sweden
[2] Physics Dept. Royal Institute of Technology, AlbaNova, 10691 Stockholm, Sweden
[3] Physikalisches Institute, Auf der Morgenstelle 14, 72076 Tuebingen, Germany
[4] IPNAS (Bât. B 15), Université de Liège, Sart Tilman, 4000 Liège 1, Belgium
and
Astrophysique et Spectroscopie, Université de Mons-Hainaut, 7000 Mons, Belgium

Received 29 October 2003 / Received in final form 16 January 2004
Published online 30 March 2004 – © EDP Sciences, Società Italiana di Fisica, Springer-Verlag 2004

Abstract. We report on a calculation of five lifetimes of metastable levels in Ar II, obtained with a relativistic Hartree-Fock method in which most of the intravalence correlation is represented within a configuration interaction scheme while core-valence correlation is described by a core-polarization model potential with a core-penetration corrective term. The quality of the calculation has been assessed through an experimental determination of the radiative lifetime of the metastable $3d\ ^4\mathrm{F}_{9/2}$ level. The experiment was performed with a laser probing technique on a stored ion beam at the CRYRING of Stockholm.

PACS. 31.10.+z Theory of electronic structure, electronic transitions, and chemical binding – 32.70.Cs Oscillator strengths, lifetimes, transition moments

1 Introduction

Metastable states can decay radiatively only by forbidden transitions. Such radiative decay may occur through magnetic dipole (M1), electric quadrupole (E2) and sometimes magnetic quadrupole (M2) or even electric octupole (E3) transitions. In general, the forbidden transitions are extremely weak compared to the other radiative transitions (E1) in the same atomic system. While a "normal" excited state in a neutral or a lowly charged ion has a lifetime of a few nanoseconds, a metastable state may live for milliseconds or even seconds. This fact makes direct observations of such radiative decays generally very difficult. Consequently, different tools, sometimes very sophisticated, for observing long lived states have been developed. Our method uses the ion beam storage ring of Stockholm University (i.e. the CRYRING [1]) utilizing a laser probing technique (LPT) for investigating the population decay of these metastable states.

Studies of metastable states are of great importance for the understanding of atomic structure of atoms or ions. Due to the very narrow natural line width of the transitions emitted from metastable levels, some forbidden transitions are strong candidates for the development of new very accurate atomic clocks. Furthermore, the forbidden transitions can dominate the emission line spectra from dilute astrophysical plasmas [2] where the metastable levels are not collisionally deexcited. Often, and this is the case in astrophysics, not only the wavelength and the assignment of transitions are needed for spectral analysis, but also the transition rates, the oscillator strengths or even the lifetimes if the corresponding branching fractions have been determined. The lifetime of a level is the inverse sum of the transition probabilities for all possible decay channels. In the theoretical treatment, such emission lines are very sensitive to subtle effects like the mixing of the levels and the corresponding lifetimes appear as a challenge for the theoreticians.

For experimental studies of radiative lifetimes of metastable levels, there are two particularly important aspects to take into account. Firstly, the observation time of the ion (or atom) has to be sufficiently long compared to the natural lifetime. Secondly, the collisional destruction must be small or negligible to permit accurate measurements of radiative decays. In this paper, we describe briefly the method we have developed at CRYRING (Stockholm), which resembles the laser probing technique adopted in ion traps. We use, however, fast ion beams and, since the LPT is applied in a collinear geometry, high resolution is achieved. This high spectral resolution, combined with the long observation time provided by the storage ring, opens the way to studies of metastable lifetimes. In the present paper, we report on an experimental lifetime measurement for the metastable $3d\ ^4\mathrm{F}_{9/2}$ level of Ar II and compare this result with our theoretical calculations. The lifetimes of other metastable levels have been calculated as well and they are also reported.

[a] e-mail: mannervik@physto.se

Finally, it should be mentioned that, although metastable levels are important for the collisional processes inside an argon ion laser, only allowed transitions have been investigated so far in the literature both experimentally and theoretically [3–6,8] and, until now, no forbidden transitions have been studied in this ion.

2 Calculations of lifetimes for metastable levels in Ar II

The ground-state levels of Ar II are $3s^2 3p^5\ ^2\mathrm{P}^\circ_{3/2}$ and $^2\mathrm{P}^\circ_{1/2}$ and the first excited even configurations are $3s3p^6$, $3s^2 3p^4(^3\mathrm{P},\ ^1\mathrm{D})nl$ with $nl = 3d$ and $4s$. The lowest metastable states are $3s^2 3p^4(^3\mathrm{P})3d\ ^4\mathrm{F}_{9/2,7/2}$ (at 142186.3 and 142717.1 cm^{-1}), $3s^2 3p^4(^3\mathrm{P})3d\ ^2\mathrm{F}_{7/2}$ (at 149179.2 cm^{-1}) and $3s^2 3p^4(^1\mathrm{D})3d\ ^2\mathrm{G}_{9/2,7/2}$ (at 154181.5 and 154204.0 cm^{-1}). These levels can decay through M1 and E2 transitions only.

Calculation of the atomic structure of Ar II requires inclusion of configuration interaction in a detailed way. In the present work, the following configurations have been considered for the calculations: $3s3p^6 + 3p^4 3d + 3p^4 4d + 3p^4 5d + 3p^4 6d + 3p^4 7d + 3p^4 8d + 3p^4 4s + 3p^4 5s + 3p^4 6s + 3p^4 7s + 3p^4 8s + 3p^4 5g + 3p^4 6g + 3p^4 7g + 3p^4 8g + 3p^4 7i + 3p^4 8i + 3s3p^4 4s^2 + 3s3p^4 4p^2 + 3s3p^4 3d^2 + 3s3p^4 4d^2 + 3s3p^5 4p + 3s3p^5 5p + 3s3p^5 4f + 3s3p^5 5f + 3p^6 3d + 3p^6 4d + 3p^6 5d + 3p^6 4s + 3p^6 5s + 3p^6 5g$. The Rydberg series were limited to $n = 8$ but the effects of additional terms, along the series, on the calculated lifetimes obtained here was found negligible.

The relativistic Hartree-Fock approach (HFR) developed by Cowan was considered for calculating the wave functions and the transition probabilities [9]. The method can be used in an ab initio way but, in addition to the explicit consideration of the interactions between the above configurations, a least-squares fit procedure can be applied allowing to get a better agreement between the experimentally determined energy levels and the calculated eigenvalues. This procedure was followed here. The experimental energy levels were taken from the NIST compilation [10]. The Slater integrals and configuration interaction parameters for the configurations not experimentally determined were multiplied by 0.85, this procedure allowing to take partly into account the interactions with many configurations which are not explicitly introduced in the above model. This procedure is well established (see e.g. [7]) and the background for its justification is provided in Cowan's book (Ref. [9], pp. 464–465).

The M1 and E2 contributions to the lifetimes of the 5 metastable levels here above quoted are given in Table 1. In this table, the summations are extended to all the possible contributions, some of them being very weak. The corresponding lifetimes are given in the last column of the same table.

We report also in Tables 2 and 3 the detailed results for the most intense transitions ($\log gf < -10.0$). It has been observed that for most of these transitions, the cancellation effects in the calculation of the line strengths do not play a role. In Figure 1, the strongest decay channels for the $3d\ ^4\mathrm{F}_{9/2}$ level, studied experimentally, are indicated.

Table 1. Ar II: contributions to the lifetimes of the metastable levels (the summations are extended to all the M1 and E2 contributions).

Energy (cm^{-1})	Level	$\sum A$ (s^{-1})	τ (s)
142186.3	$3s^2 3p^4(^3\mathrm{P})3d\ ^4\mathrm{F}_{9/2}$	3.135×10^{-02} (M1)	4.35
		1.984×10^{-01} (E2)	
142717.1	$3s^2 3p^4(^3\mathrm{P})3d\ ^4\mathrm{F}_{7/2}$	2.455×10^{-02} (M1)	4.45
		2.000×10^{-01} (E2)	
149179.2	$3s^2 3p^4(^3\mathrm{P})3d\ ^2\mathrm{F}_{9/2}$	8.386×10^{-02} (M1)	1.25
		7.173×10^{-01} (E2)	
154204.0	$3s^2 3p^4(^1\mathrm{D})3d\ ^2\mathrm{G}_{7/2}$	1.304×10^{-01} (M1)	6.10
		3.343×10^{-02} (E2)	
154181.5	$3s^2 3p^4(^1\mathrm{D})3d\ ^2\mathrm{G}_{9/2}$	1.812×10^{-01} (M1)	4.90
		2.291×10^{-02} (E2)	

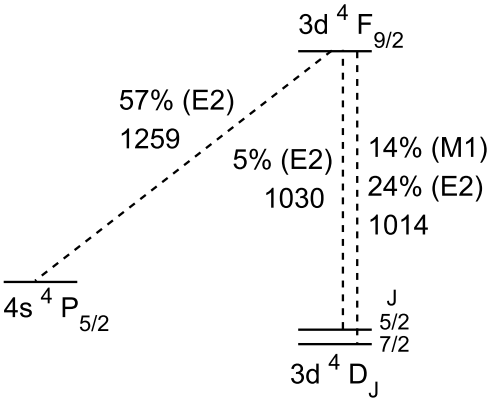

Fig. 1. Schematic figure showing the forbidden transitions from the metastable $3d\ ^4\mathrm{F}_{9/2}$-level. The relative transition probabilities, according to the HFR calculations, are given in percent and the wavelengths in nm.

3 Experiment

The experiment was performed at the ion storage ring CRYRING at the Manne Siegbahn Laboratory in Stockholm. The Ar^+ ions were produced in a low voltage hot cathode ion source (MINIS) and then accelerated to 40 keV. The Ar^+ beam was deflected in a 90° magnet and the different isotopes were well separated. The $^{40}Ar^+$ isotope was selected and the ions were then transported and injected into the storage ring with a beam current of a few microamperes, or approximately 10^{10} ions. The ions were stored at injection energy and at the base pressure of less than 1×10^{-11} Torr, the lifetime of the stored ion beam was on the order of one minute. The decay, due to neutralization in collisions with rest gas, was monitored with a scintillator detector connected to a multiscaler and also by a current transformer to obtain the absolute current.

Table 2. Ar II most intense ($\log gf > -10.0$) forbidden transitions, M1 contributions.

Transition	$\log gf$	gA (s^{-1})
$3s^2 3p^4(^3\mathrm{P})3d\ ^4\mathrm{D}_{7/2}$ — $3s^2 3p^4(^3\mathrm{P})3d\ ^4\mathrm{F}_{9/2}$	−8.40	3.13×10^{-01}
$3s^2 3p^4(^3\mathrm{P})3d\ ^4\mathrm{D}_{7/2}$ — $3s^2 3p^4(^3\mathrm{P})3d\ ^4\mathrm{F}_{7/2}$	−8.73	1.56×10^{-01}
$3s^2 3p^4(^3\mathrm{P})3d\ ^4\mathrm{D}_{5/2}$ — $3s^2 3p^4(^3\mathrm{P})3d\ ^4\mathrm{F}_{7/2}$	−9.60	2.07×10^{-02}
$3s^2 3p^4(^3\mathrm{P})3d\ ^4\mathrm{F}_{9/2}$ — $3s^2 3p^4(^3\mathrm{P})3d\ ^4\mathrm{F}_{7/2}$	−6.77	1.95×10^{-02}
$3s^2 3p^4(^3\mathrm{P})3d\ ^4\mathrm{D}_{7/2}$ — $3s^2 3p^4(^3\mathrm{P})3d\ ^2\mathrm{F}_{7/2}$	−8.69	4.24×10^{-01}
$3s^2 3p^4(^3\mathrm{P})3d\ ^4\mathrm{D}_{5/2}$ — $3s^2 3p^4(^3\mathrm{P})3d\ ^2\mathrm{F}_{7/2}$	−9.22	1.22×10^{-01}
$3s^2 3p^4(^3\mathrm{P})3d\ ^4\mathrm{F}_{9/2}$ — $3s^2 3p^4(^3\mathrm{P})3d\ ^2\mathrm{F}_{7/2}$	−8.63	7.25×10^{-02}
$3s^2 3p^4(^3\mathrm{P})3d\ ^4\mathrm{F}_{7/2}$ — $3s^2 3p^4(^3\mathrm{P})3d\ ^2\mathrm{F}_{7/2}$	−9.30	1.35×10^{-02}
$3s^2 3p^4(^3\mathrm{P})3d\ ^4\mathrm{F}_{5/2}$ — $3s^2 3p^4(^3\mathrm{P})3d\ ^2\mathrm{F}_{7/2}$	−8.82	3.65×10^{-02}
$3s^2 3p^4(^1\mathrm{D})3d\ ^2\mathrm{D}_{5/2}$ — $3s^2 3p^4(^3\mathrm{P})3d\ ^2\mathrm{F}_{7/2}$	−8.91	2.51×10^{-03}
$3s^2 3p^4(^3\mathrm{P})3d\ ^4\mathrm{F}_{9/2}$ — $3s^2 3p^4(^1\mathrm{D})3d\ ^2\mathrm{G}_{7/2}$	−9.46	3.11×10^{-02}
$3s^2 3p^4(^3\mathrm{P})3d\ ^4\mathrm{F}_{7/2}$ — $3s^2 3p^4(^1\mathrm{D})3d\ ^2\mathrm{G}_{7/2}$	−8.31	4.11×10^{-01}
$3s^2 3p^4(^3\mathrm{P})3d\ ^4\mathrm{F}_{5/2}$ — $3s^2 3p^4(^1\mathrm{D})3d\ ^2\mathrm{G}_{7/2}$	−8.43	2.93×10^{-01}
$3s^2 3p^4(^3\mathrm{P})3d\ ^2\mathrm{F}_{7/2}$ — $3s^2 3p^4(^1\mathrm{D})3d\ ^2\mathrm{G}_{7/2}$	−7.82	2.38×10^{-01}
$3s^2 3p^4(^3\mathrm{P})3d\ ^2\mathrm{F}_{5/2}$ — $3s^2 3p^4(^1\mathrm{D})3d\ ^2\mathrm{G}_{7/2}$	−8.28	5.73×10^{-02}
$3s^2 3p^4(^3\mathrm{P})3d\ ^4\mathrm{F}_{9/2}$ — $3s^2 3p^4(^1\mathrm{D})3d\ ^2\mathrm{G}_{9/2}$	−7.85	$1.29 \times 10^{+00}$
$3s^2 3p^4(^3\mathrm{P})3d\ ^4\mathrm{F}_{7/2}$ — $3s^2 3p^4(^1\mathrm{D})3d\ ^2\mathrm{G}_{9/2}$	−8.35	3.79×10^{-01}
$3s^2 3p^4(^3\mathrm{P})3d\ ^2\mathrm{F}_{7/2}$ — $3s^2 3p^4(^1\mathrm{D})3d\ ^2\mathrm{G}_{9/2}$	−8.06	1.39×10^{-01}

Table 3. Ar II most intense ($\log gf > -10.0$) forbidden transitions, E2 contributions.

Transition	$\log gf$	gA (s^{-1})
$3s^2 3p^4(^3\mathrm{P})3d\ ^4\mathrm{D}_{7/2}$ — $3s^2 3p^4(^3\mathrm{P})3d\ ^4\mathrm{F}_{9/2}$	−8.15	5.59×10^{-01}
$3s^2 3p^4(^3\mathrm{P})3d\ ^4\mathrm{D}_{5/2}$ — $3s^2 3p^4(^3\mathrm{P})3d\ ^4\mathrm{F}_{9/2}$	−8.81	1.18×10^{-01}
$3s^2 3p^4(^3\mathrm{P})4s\ ^4\mathrm{P}_{5/2}$ — $3s^2 3p^4(^3\mathrm{P})3d\ ^4\mathrm{F}_{9/2}$	−7.59	$1.31 \times 10^{+00}$
$3s^2 3p^4(^3\mathrm{P})3d\ ^4\mathrm{D}_{3/2}$ — $3s^2 3p^4(^3\mathrm{P})3d\ ^4\mathrm{F}_{7/2}$	−8.70	1.63×10^{-01}
$3s^2 3p^4(^3\mathrm{P})4s\ ^4\mathrm{P}_{3/2}$ — $3s^2 3p^4(^3\mathrm{P})3d\ ^4\mathrm{F}_{7/2}$	−7.96	5.00×10^{-01}
$3s^2 3p^4(^3\mathrm{P})3d\ ^4\mathrm{D}_{7/2}$ — $3s^2 3p^4(^3\mathrm{P})3d\ ^4\mathrm{F}_{7/2}$	−8.58	2.21×10^{-01}
$3s^2 3p^4(^3\mathrm{P})3d\ ^4\mathrm{D}_{5/2}$ — $3s^2 3p^4(^3\mathrm{P})3d\ ^4\mathrm{F}_{7/2}$	−8.54	2.40×10^{-01}
$3s^2 3p^4(^3\mathrm{P})4s\ ^4\mathrm{P}_{5/2}$ — $3s^2 3p^4(^3\mathrm{P})3d\ ^4\mathrm{F}_{7/2}$	−8.06	4.77×10^{-01}
$3s^2 3p^4(^3\mathrm{P})4s\ ^4\mathrm{P}_{3/2}$ — $3s^2 3p^4(^3\mathrm{P})3d\ ^2\mathrm{F}_{7/2}$	−8.81	2.19×10^{-01}
$3s^2 3p^4(^3\mathrm{P})4s\ ^2\mathrm{P}_{3/2}$ — $3s^2 3p^4(^3\mathrm{P})3d\ ^2\mathrm{F}_{7/2}$	−7.20	$5.51 \times 10^{+00}$
$3s^2 3p^4(^3\mathrm{P})3d\ ^2\mathrm{P}_{3/2}$ — $3s^2 3p^4(^3\mathrm{P})3d\ ^2\mathrm{F}_{7/2}$	−9.76	2.03×10^{-03}
$3s^2 3p^4(^3\mathrm{P})4s\ ^2\mathrm{P}_{3/2}$ — $3s^2 3p^4(^1\mathrm{D})3d\ ^2\mathrm{G}_{7/2}$	−9.40	7.00×10^{-02}
$3s^2 3p^4(^1\mathrm{D})3d\ ^2\mathrm{D}_{3/2}$ — $3s^2 3p^4(^1\mathrm{D})3d\ ^2\mathrm{G}_{7/2}$	−8.31	1.61×10^{-01}
$3s^2 3p^4(^1\mathrm{D})4s\ ^2\mathrm{D}_{3/2}$ — $3s^2 3p^4(^1\mathrm{D})3d\ ^2\mathrm{G}_{7/2}$	−9.23	4.09×10^{-03}
$3s^2 3p^4(^1\mathrm{D})3d\ ^2\mathrm{D}_{5/2}$ — $3s^2 3p^4(^1\mathrm{D})3d\ ^2\mathrm{G}_{7/2}$	−9.13	2.14×10^{-02}
$3s^2 3p^4(^1\mathrm{D})3d\ ^2\mathrm{D}_{5/2}$ — $3s^2 3p^4(^1\mathrm{D})3d\ ^2\mathrm{G}_{9/2}$	−8.15	2.06×10^{-01}
$3s^2 3p^4(^1\mathrm{D})4s\ ^2\mathrm{D}_{5/2}$ — $3s^2 3p^4(^1\mathrm{D})3d\ ^2\mathrm{G}_{9/2}$	−9.29	3.07×10^{-03}

The laser system consists of a Coherent 699-29 autoscan ring dye laser pumped by a Coherent Innova 400-25 argon ion laser. The dye DCM was used to obtain laser light of the desired wavelength and with a sufficient output power of ∼300 mW. The laser probing pulses were created with a mechanical shutter, Uniblitz LS6, controlled by the data acquisition system to set the increasing delay from the injection of ions into CRYRING. A telescope and a system of mirrors were used to transport the laser beam into the storage ring, in order to overlap collinearly with the ion beam. The ion beam was locally accelerated with a set of cylindrical electrodes set on a negative high voltage of −2 kV, in order to Doppler shift the ions into laser resonance [11] in front of the Hamamatsu R585 photomultiplier tube. The laser beam was focused to a diameter of approximately 10 mm in front of the detector, which has the same size as the photocathode on the PM-tube. A set of lenses was used to obtain a 1:1 image of

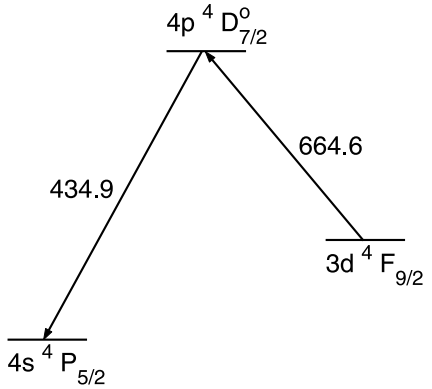

Fig. 2. Schematic figure showing the levels and transitions that are involved in the present lifetime experiment. The 664.6 nm transition was induced with laser light and fluorescence light from the 434.9 nm decay channel was observed.

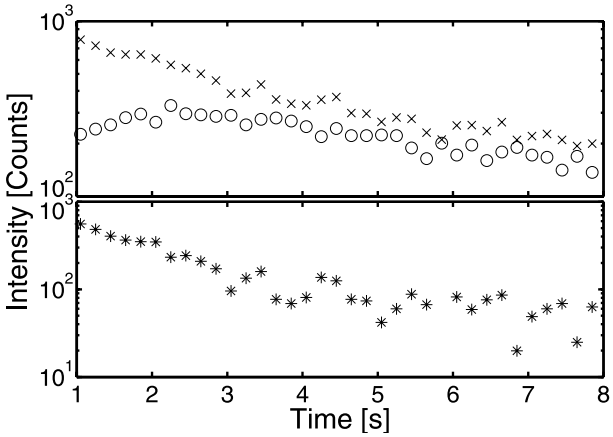

Fig. 3. Plot of the repopulation correction required for accurate lifetime determination. In the upper part of the figure, the raw data (crosses) and the repopulation (open circles) are obtained separately with the laser probing technique. In the lower part, the raw data are corrected for repopulation.

the laser-induced fluorescence on the PM-tube. A colored glass filter was used to reduce background of scattered laser light. The background was about 5–10 s^{-1} with the laser on.

A VME-based data acquisition system was used to control the laser probe pulses and to collect data. Laser Probing used the transitions illustrated in Figure 2. Every set of data consists of one lifetime curve of the selected metastable level, one ion beam current decay curve and four different normalization curves in order to observe any possible fluctuations during the measurement [12].

4 Measurements

With a laser it is possible to induce the transition from the metastable $3d\ ^4F_{9/2}$ level to the short lived $4p\ ^4D^\circ_{7/2}$ state. The ions excited to the short lived state can decay spontaneously by a radiative transition down to the $4s\ ^4P_{5/2}$ state, emitting photons of wavelength 434.9 nm (see Fig. 2). This fluorescence intensity is proportional to the population of the metastable level at the time when the laser light is applied. The process is destructive (since the population of the metastable level is quenched by the laser) and, consequently, the probe pulse can only be applied once every ring cycle and the data collection time for a lifetime curve was then about 3 hours in this case.

To measure the efficiency of the outpumping process of the metastable level, the ions were exposed resonantly to laser light while a multiscaler recorded the fluorescence light as a function of time [11]. After 100 ms, only a few percent of the original metastables were left. The duration of the laser probe pulse was then fixed to be 200 ms, yielding 100−200 counts recorded per prompt probe pulse. The detector background of 5−10 s^{-1} thus gave a contribution of approximately 1 count for each 200 ms interval. By introducing a variable delay time between injection and the resonant laser pulse, the decay of the selected metastable level could be probed selectively. The delay was stepwise changed with an increment Δt for each ring cycle, and by recording the number of fluorescence counts, for each delay, the lifetime curve was obtained [11,12].

We have previously observed collisional excitation of ground state ions to the metastable states during the ion storage [13]. This repopulation of the measured metastable level changes the shape of the observed lifetime curve significantly. We have, however, developed a technique to record the repopulation process separately [13] which allows subtraction of this effect [11,12].

The metastable level is populated already in the ion source. To observe repopulation of the metastable state a laser pulse is required to quench the ions in the metastable level that were populated in the ion source. After a certain delay from the quench pulse, a regular probe pulse is added in order to measure the repopulation of the selected metastable level. The delay between the quench pulse and probe pulse is stepwise changed until a repopulation curve is obtained [13] (Fig. 3).

5 Results and discussion

Each measurement yields raw data consisting of five different curves, three of them being used for normalization. All the curves are required to exclude all potential sources of systematical errors.

In LPT only one point on the decay curve is recorded for each ion injection. Instability of production of metastable ions inside the ion source would be a significant source of uncertainty. It could change the metastable fraction between different ring cycles. To avoid the effect of such fluctuations, a normalization is done [12]. The observed effect was, however, smaller than the statistical deviation deduced from the experiment.

Another systematic effect is that the ions may be excited by collisions with molecules in the rest gas (as discussed above). This effect gives rise to a tail in the decay curve with a slope corresponding to the loss of ground

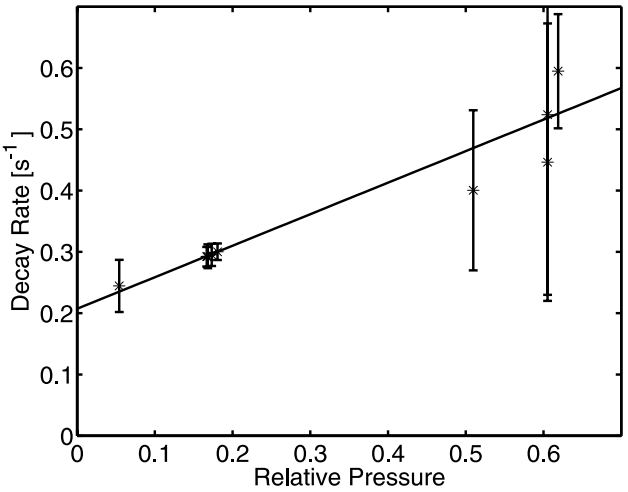

Fig. 4. The final lifetime was extracted out of the Stern-Vollmer plot, illustrating the decay rate versus the pressure in the storage ring. Extrapolation of the fitted line to zero pressure gave the decay rate without contributions from collisional quenching, i.e. the radiative lifetime.

state particles. In this tail there is balance between decay and excitation. This effect, denoted repopulation, was subtracted. The repopulation correction for this experiment changed the extracted lifetimes significantly, almost 25%.

The corrected decay curve yields the decay of the ions in the metastable level that were excited in the ion source. This curve reflects both the radiative decay and the collisional quenching. We have

$$\frac{1}{\tau_{meas}} = \frac{1}{\tau_{rad}} + \frac{1}{\tau_{quench}} \qquad (1)$$

i.e. the measured decay rate ($1/\tau_{meas}$) is the sum of natural radiative decay rate and the destruction rate (of collisional quenching). The destructive rate depends linearly on the background pressure, and, by lifetimes measurements at different pressures and extrapolation down to zero pressure, the pure radiative lifetime was obtained. It was graphically deduced from a Stern-Vollmer plot, see Figure 4. The changes in pressure were achieved by heating one of the non-evaporative getter pumps with an external heater. It was found that approximately 30% of the decay during lifetime measurements at base pressure was due to collisional quenching.

The extracted radiative lifetime of the $3d\,^4\mathrm{F}_{9/2}$ level in Ar II was finally determined to be $\tau = 4.9 \pm 0.7$ s. The error is composed of the statistical error from the fitted curves, the uncertainly due to statistical spread between different measurements as well as the uncertainty in the correction for repopulation, fluorescence normalization and, in particular, for collisional quenching. Our calculations by the relativistic Hartree-Fock approach gave a lifetime of 4.35 s for the measured metastable level, which is in good agreement with experiment. This agreement suggests that our results for other metastable levels in Ar II probably are reliable.

6 Conclusion

We present the first investigation of the radiative decay of metastable levels in Ar II. Five calculated radiative lifetimes and one experimental value are reported. The agreement between experiment and theory, for the metastable $^4\mathrm{F}_{9/2}$ level, is good and gives some weight to the theoretical model adopted in the present work.

EB is Research Director of the Belgian National Fund for Scientific Research (FNRS). Financial support from this organization is acknowledged. This work was also supported by the Swedish Research Council (VR). We are also grateful to the staff of the CRYRING facility and appreciate their effort to provide stable laboratory conditions.

References

1. K. Abrahamsson, G. Andler, L. Bagge, E. Beebe, P. Carlé, H. Danared, S. Egnell, K. Ehrnstén, M. Engström, C.J. Herrlander, J. Hilke, J. Jeansson, A. Källberg, S. Leontein, L. Liljeby, A. Nilsson, A. Paal, K.-G. Rensfelt, U. Rosengård, A. Simonsson, A. Soltan, J. Starker, M. af Ugglas, Nucl. Instr. Meth. Phys. Meth. Phys. Res. B **79**, 268 (1993)
2. H. Hartman, A. Derkatch, M.P. Donnelly, T. Gull, A. Hibbert, S. Johansson, H. Lundberg, S. Mannervik, L.-O. Norlin, D. Rostohar, P. Royen, P. Schef, Astron. Astrophys. **397**, 1143 (2003)
3. W.L. Wiese, M.W. Smith, B.M. Miles, in *Atomic Transition Probabilities II* (Washington DC, US Govt Printing Office, 1969)
4. H. Schmoranzer, P. Hartmetz, D. Marger, J. Phys. B: At. Mol. Phys. **19**, 1023 (1986)
5. D. Marger, H. Schmoranzer, Phys. Lett. A **150**, 196 (1990)
6. V. Vujnović, W.L. Wiese, Phys. Chem. Ref. Data **21**, 919 (1992)
7. E. Biémont, C. Froese Fischer, M.R. Godefroid, P. Palmeri, P. Quinet, Phys. Rev. A **62**, 032512 (2000)
8. A. Hibbert, J.E. Hansen, J. Phys. B: At. Mol. Opt. Phys. **27**, 3325 (1994)
9. R.D. Cowan, *The Theory of Atomic Structure and Spectra* (University of California Press, Berkeley, 1981)
10. N.I.S.T. Atomic Spectra Database 2.0, `http://physics.nist.gov/cgi-bin/AtData/main-asd` (2003)
11. J. Lidberg, A. Al-Khalili, L.-O. Norlin, P. Royen, X. Tordoir, S. Mannervik, Nucl. Instrum. Meth. Phys. Res. B **152**, 157 (1999)
12. S. Mannervik, Phys. Scripta **T105**, 67 (2003)
13. S. Mannervik, J. Lidberg, L.O. Norlin, P. Royen, Phys. Rev. A **56**, R1075 (1997)